Noname manuscript No.
(will be inserted by the editor)

Sensitivity of idealised baroclinic waves to mean atmospheric temperature and meridional temperature gradient changes

Mika Rantanen · Jouni Räisänen · Victoria A. Sinclair · Heikki Järvinen

Received: date / Accepted: date

Abstract The sensitivity of idealised baroclinic waves to different atmospheric temperature changes is studied. The temperature changes are based on those which are expected to occur in the Northern Hemisphere with climate change: 1) uniform temperature increase, 2) decrease of the lower level meridional temperature gradient, and 3) increase of the upper level temperature gradient. Three sets of experiments are performed, first without atmospheric moisture, thus seeking to identify the underlying adiabatic mechanisms which drive the response of extra-tropical storms to changes in the environmental temperature. Then, similar experiments are performed in a more realistic, moist environment, using fixed initial relative humidity distribution. Warming the atmosphere uniformly tends to decrease the kinetic energy of the cyclone, which is linked both to a weaker capability of the storm to exploit the available potential energy of the zonal mean flow, and less efficient production of eddy kinetic energy in the wave. Unsurprisingly, the decrease of the lower level temperature gradient weakens the resulting cyclone regardless of the presence of moisture. The increase of the temperature gradient in the upper troposphere has a more complicated influence on the storm dynamics: in the dry atmosphere the maximum eddy kinetic energy decreases, whereas in the moist case it increases. Our analysis suggests that the slightly unexpected decrease of eddy kinetic energy in the dry case with an increased upper tropospheric temperature gradient originates from the weakening of the meridional heat flux by the eddy. However, in the more realistic moist case, the diabatic heating enhances the interaction between upper- and low-level potential vorticity anomalies and hence helps the surface cyclone to exploit the increased upper level baroclinicity.

Keywords WRF model · Idealised simulation · Extratropical cyclone · Energy conversion

M. Rantanen · J. Räisänen · V. A. Sinclair · H. Järvinen
Institute for Atmospheric and Earth System Research / Physics
P.O. Box 64 (Gustaf Hällströmin katu 2a) FI-00014
University of Helsinki, Finland
E-mail: mika.p.rantanen@helsinki.fi

1 Introduction

Extra-tropical cyclones are ubiquitous in the mid-latitude atmosphere, occurring most frequently during the winter season. They affect our everyday life by inducing variations and extremes of weather, sometimes with severe impacts to the society (e.g. Wernli et al, 2002; Fink et al, 2009). Extra-tropical cyclones also transport large amounts of heat and momentum, and are thus an important component of the atmospheric general circulation.

A large number of previous studies have investigated the changes in the intensity (e.g. Bengtsson et al, 2009), frequency (e.g. Lambert and Fyfe, 2006; Zappa et al, 2013), and tracks (e.g. Yin, 2005; Bengtsson et al, 2006) of extra-tropical cyclones in a warmer climate. All of these changes in cyclone characteristics partly result from the different atmospheric temperature distribution in the future climate. For example, climate change projections made with General Circulation Models (GCM) suggest that in mid-latitudes, the meridional low-level temperature gradient will decrease whereas the gradient at upper levels will increase (Woollings, 2008; Catto et al, 2011).

One widely used method for studying the dynamics of extra-tropical cyclones is idealised simulations (e.g. Fantini, 2004; Boutle et al, 2010, 2011; Booth et al, 2013; Blázquez et al, 2013; Kirshbaum et al, 2018). One specific example is the baroclinic lifecycle simulation, in which only one low pressure system is simulated. This technique allows one to explore the changes in extra-tropical cyclone dynamics much

more easily than the simulations created using e.g. complex Earth System models. Most of the recent studies carried out with idealised baroclinic wave simulations have investigated the effect of atmospheric moisture on cyclone characteristics. For instance, Boutle et al (2010) studied the dry and moist boundary layer structure and vertical transport of moisture within the idealised cyclone. They found that the kinetic energy of the storm was doubled with the inclusion of moisture. Furthermore, the changes in cyclone dynamics and intensity with increased atmospheric moisture content have been studied in detail by Booth et al (2013). The robust result in that study was that nearly all the important metrics of storm strength increase when the moisture is increased.

However, less emphasis has been given to studying how changes in the large-scale temperature distribution, as anticipated for the future climate, affect the strength and development of numerically simulated cyclones in idealised cases. Boutle et al (2011) studied the sensitivity of moisture transport by idealised cyclones to some large-scale environmental variables, such as initial relative humidity, absolute temperature, and the meridional temperature gradient and thus the strength of the zonal jet. They concluded that relative humidity has little impact on the ability of a cyclone to transport moisture, whereas the absolute temperature and its meridional gradient provide much stronger controls. They, however, did not focus on the mechanisms by which the change of temperature and its gradient affect the dynamics and intensity of the storm.

The sensitivity of idealised moist baroclinic waves to environmental temperature and moisture content was studied by Kirshbaum et al (2018). They initialized the model runs with different mean surface temperatures, varying between 275–290 K, and found that the eddy kinetic energy did not increase at larger temperatures due to unfavourable phasing between vertical motion and buoyancy within the warm sector. Another methodological novelty of their study was that the model domain was much larger in the zonal direction (L_x = 16000 km) than typically used in baroclinic life cycle experiments (e.g Boutle et al (2010) used L_x = 4000 km) and that two types of simulations were performed: one set using a single domain-centered initial perturbation and the second set using three equally spaced perturbations. The simulations initialised with three perturbations show a different response to the environmental temperature than than simulations with a single perturbation as the wave was found to interact negatively with itself. Thus, Kirshbaum et al (2018) conclude that periodic waves exhibited faster decrease in intensity at larger temperatures compared to isolated waves, which had not been documented previously.

Very recently, Tierney et al (2018) reported how extratropical cyclones respond to changes in baroclinicity and temperature in an idealized environment. This study was an important addition to the existing literature, as the changes in baroclinicity have received relatively little attention amongst recent idealized studies. Tierney et al (2018) changed simultaneously both the baroclinicity and the bulk temperature of the cyclone environment, and thus discovered the relative effects of these two factors to the cyclone intensity.

In general, the main consensus among the recent studies is an amplification of the storm when the moisture content is increased from zero to typical present-day values (Boutle et al, 2010; Booth et al, 2013; Kirshbaum et al, 2018; Tierney et al, 2018). However, increasing the atmospheric moisture further from the present-day values has led to partly contradictory results in previous idealised experiments. For example, keeping the relative humidity fixed, Boutle et al (2011) found that the eddy kinetic energy tends to increase with increasing atmospheric temperature. A similar result was found in Whitaker and Davis (1994), who reported more rapid cyclogenesis when the mean surface temperature was increased by 10 K. However, inconsistent with these two studies, the main conclusion of Kirshbaum et al (2018) was that the increase of temperature with constant relative humidity makes the storm weaker. In addition, Tierney et al (2018) documented the non-monotonic behavior of the storm intensity with increasing temperature, regardless of the magnitude of baroclinicity. These two outcomes are in agreement with recent idealised aqua-planet GCM studies, where the sensitivity of eddy kinetic energy to global mean atmospheric temperature has been studied: O'Gorman (2011) and Pfahl et al (2015) show that with present-day temperature values the eddy kinetic energy is very close to its maximum, and tends to decrease with further warming.

Nonetheless, in addition to increased moisture content, changes in the meridional temperature gradient with changing climate are also expected to impact the development of baroclinic eddies. Thus, the main objective of this paper is to study the sensitivity of extra-tropical cyclones to meridional temperature gradient changes. Since opposing changes in the temperature gradient are expected to occur in the Northern Hemisphere at lower and upper levels (Woollings, 2008), the effects of the lower and upper level changes are studied separately. Before that, the response of the simulated midlatitude cyclone to an uniform increase of temperature is reported. This experiment of uniform warming is included in our paper to address the three different temperature forcings predicted to occur in the warmer climate: 1) uniform increase of atmospheric temperature, 2) decreased lower level temperature gradient and 3) increased upper level temperature gradient. Based on earlier, slightly contradictory results, we cannot formulate a clear hypothesis of how the uniform increase of temperature will affect to the intensity of the storm. On the other hand, we would expect that the changes in lower level and upper level temperature gradient will have opposing effects on the intensity of the cyclone, due to their opposing effects on atmospheric baro-

clinicity. To assess the changes in the adiabatic dynamics of cyclones, the experiments are first conducted without atmospheric moisture. After that, the experiments are repeated in a moist environment.

First, in Section 2, the model set-up, the experiments and the energy metrics used in this paper are described. Then, the results of our experiments are reported in Section 3, which is divided to three subsections, according to the three temperature experiments. A brief discussion of some pertinent issues arising from the results is then given in Section 4. Finally, in Section 5, the main conclusions of the study are reported.

2 Methods

2.1 The model

We used the Weather Research and Forecast (WRF) model v. 3.8.1 (Shamarock et al, 2008), in its idealized mode in a Cartesian geometry. The model configuration was a periodic channel, with symmetric north-south boundaries and periodic east-west boundaries. The simulations were run for 10 days, in a domain of 5000 km x 8000 km x 16 km, in the x, y and z directions, respectively. The horizontal grid spacing in our study was 50 km. We tested different zonal wavelengths, and thus different zonal domain sizes, varying between 3500 and 6000 km. 5000 km was finally chosen because the longest wavelengths were found to generate unwanted secondary lows, whereas wavelengths shorter than 5000 km produced a less deep cyclone. Although Kirshbaum et al (2018) used a much wider domain in the zonal direction, our choice of domain is more closely comparable with the domains used in other baroclinic wave studies. In the vertical direction, 64 sigma levels were used. The pressure at the model top varied between 125 and 100 hPa, depending on the experiment and location in south-north direction. After running the simulations, the model output data were interpolated to 19 evenly spaced pressure levels, from 1000 hPa to 100 hPa. Thus, a small part of our data at the upper boundary were extrapolated above the model top. The Coriolis parameter was held constant, with value of $10^{-4}\ s^{-1}$, corresponding to the real value at the latitude $\phi = 43^{\circ}$.

Cloud microphysics were parameterized using the WSM3 scheme (Hong et al, 2004), which has 3-class microphysics (raindrops, cloud droplets and water vapor) for liquid water, but assumes ice processes below the freezing point. The WSM3 scheme is relatively simple, and thus the amount, timing and location of latent heat release would potentially differ if a more complex microphysics scheme was used. For cumulus convection, the Kain-Fritsch scheme (Kain and Fritsch, 1993) was used, and the YSU scheme (Hong et al, 2006) was selected to parameterize the boundary layer turbulence. Surface fluxes were calculated using the MM5 similarity scheme (e.g. Paulson, 1970). For simplicity, the radiation scheme was switched off in our experiments. Even though this choice of neglecting radiation moves our experiments further from reality, it makes the interpretation of diabatic heating easier, leaving latent heat release as the only major source of diabatic heating in the free atmosphere.

For the model runs, we used the standard initial condition of the baroclinic test case, which is included in the WRF model package. The unperturbed initial states of zonal wind and temperature were zonally symmetric and in thermal wind balance, resembling their distributions in the Northern Hemisphere winter (Fig. 1). The same initial conditions were used e.g. by Sinclair and Keyser (2015), and the zonal jet is described in the paper of Waite and Snyder (2009). To enable others to reproduce our results, we have archived the initial condition files of our experiments, the namelist used in the WRF simulations, and a piece of WRF source code which sets up the initial conditions needed to run the model. These data are available from https://zenodo.org/record/1044980.

The evolution of the baroclinic disturbance was triggered by applying a sinusoidal temperature perturbation to the mid-tropospheric temperature field. The maximum of the initial perturbation was 1 K, located vertically at the level of 8 km and in the middle of the domain in the y-direction. The magnitude of the disturbance decreased to zero when approaching the top and the bottom of the domain. See Section S1.1 of the Supplementary material for details.

2.2 Numerical experiments

Three sets of experiments were performed. These are denoted as Experiment UNI, LOW and UP, referring to temperature forcings uniformly in the atmosphere, at lower levels, and at upper levels, respectively. Each of the experiments consisted of three numerical simulations with different amplitudes of the temperature forcing. Technically, the initial atmospheric temperature distribution was first changed. After this, the new pressure distribution was calculated, by integrating the hydrostatic equation from the bottom of the domain to the top, maintaining the surface pressure constant in all the experiments. To keep the initial state in a hydrostatic balance, new density values were calculated with the ideal gas law, using the new temperature and pressure values. Finally, the zonal wind field was adapted to the modified temperature and pressure fields by applying the geostrophic wind law. Thus, in addition to temperature, this procedure yielded slightly different initial conditions also for zonal wind speed and pressure in all three experiments. Nevertheless, the resulting initial states were in a perfect thermal wind balance and did not evolve with time when simulations were performed without the initial disturbance (not shown).

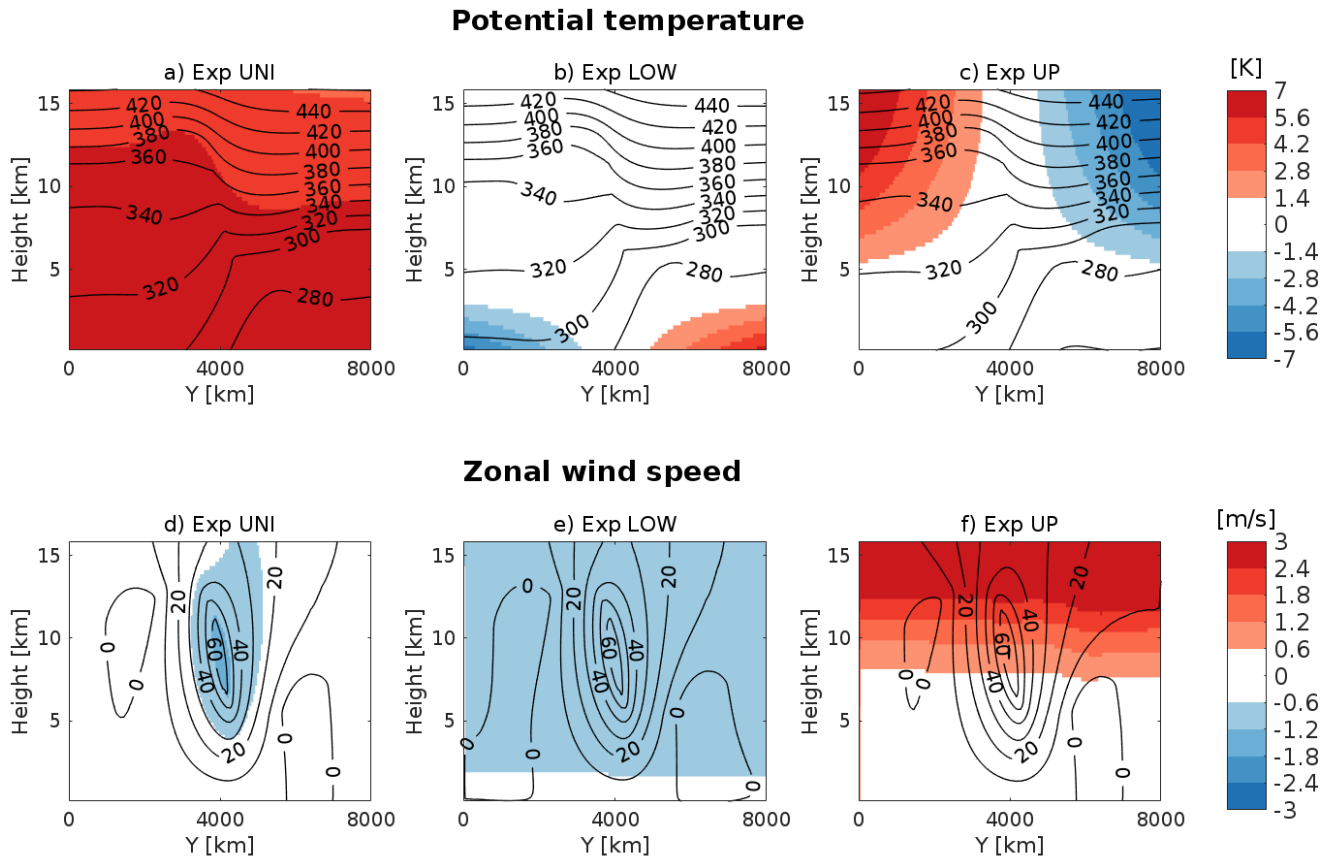

Fig. 1 Zonal mean potential temperature (contours) and differences from the control run (shading) for a) uniform temperature increase, b) the decrease of lower level temperature gradient and c) the increase of upper level temperature gradient. Figures d), e) and f) show the same experiments but for the zonal wind speed. The contours show the initial potential temperature or wind speed for the T_0 = 6 K runs and the shading shows the difference T_0 = 6 minus control

In all the numerical simulations, the same initial distribution of relative humidity was used, meaning that the moisture content of the atmosphere varied based on the temperature change. Keeping relative humidity constant is a reasonable assumption based on global climate model simulations (Solomon, 2007).

A control run (hereafter denoted as CTRL) with no temperature change was also performed. The sea surface temperature (SST) in CTRL varied from 298 K (southern boundary) to 259 K (northern boundary), being 279 K in middle of the domain, in the area where the baroclinic wave developed. In CTRL, as well as the other experiments, the SST was uniformly 0.5 K colder than the initial air temperature at the lowest model level. Thus, the SST was changed in all experiments, according to the change of the lowest level air temperature.

First, in Experiment UNI, the mean atmospheric temperature was increased uniformly everywhere in the model domain by T_0 = 2, 4 and 6 K. The initial state of the potential temperature in the T_0 = 6 K run and the difference from CTRL are shown in Fig. 1a. Note that the uniform increase was imposed to the initial temperature field, whereas Fig. 1 shows the initial potential temperature. The warming of the whole domain by 6 K caused the deceleration of the initial jet stream by up to 1.5 ms^{-1} (Fig. 1d). This was because the uniform warming made pressure increase relatively more in the northern part of the domain, which reduced the meridional pressure gradient and hence decreased the geostrophic wind speed.

In Experiment LOW, the meridional temperature gradient in the lower troposphere was decreased. The northern boundary of the model domain was warmed and the southern boundary cooled by T_0 = 2, 4 and 6 K, with a linear interpolation in-between, giving zero change in the middle of the domain. The initial temperature change as a function of the meridional coordinate (y) and pressure (p) was

$$\Delta T(y,p) = T_0 * \frac{2y-(y_n+1)}{y_n-1} * \begin{cases} \frac{p-p_{th}}{p_S-p_{th}} & \text{if } p > p_{th} \\ 0 & \text{if } p < p_{th} \end{cases}. \quad (1)$$

Here $T_0 = 2, 4$ or 6 K is the amplitude of the gradient change and $y_N = 160$ is the number of grid points in the meridional direction. The change had its maximum amplitude at the surface (pressure p_S) and was linearly reduced to zero at

the level p_{th} = 600 hPa. In the T_0 = 6 K run of Experiment LOW, the initial zonal wind speed was roughly 1 ms^{-1} reduced compared to the control run over all of the simulation domain, except at the surface (Fig. 1e), because of the decreased baroclinicity in the lower troposphere.

Thirdly, in Experiment UP, the meridional temperature gradient in the upper troposphere was increased. The implementation was analogous to Experiment LOW except for the sign of the temperature change and the layer in which it was applied:

$$\Delta T(y,p) = T_0 * \frac{(y_n+1)-2y}{y_n-1} * \begin{cases} \frac{p_{th}-p}{p_{th}-p_{TOP}} & \text{if } p < p_{th} \\ 0 & \text{if } p > p_{th} \end{cases} \quad (2)$$

where again T_0 = 2, 4 or 6 K. p_{TOP} is the pressure at the model top (at the altitude of 16 km), and p_{th} = 600 hPa. Increasing of the upper level temperature gradient by T_0 = 6 K accelerated the zonal wind speed near the top of the model domain by over 3 ms^{-1} (Fig. 1f).

In Experiment LOW at the surface and Experiment UP at the model top, the changes T_0 = 2, 4 and 6 K correspond to changes of 4, 8 and 12 K in the meridional temperature difference across the model domain. In the vertical direction, the gradient changes in both experiments were gradually attenuated to zero at the level of 600 hPa. Note that even though the thicknesses of the modified temperature layers in Experiment LOW and UP are almost equal in terms of the pressure interval, the zonal wind speed change in Experiment UP was notably larger, due to the lower density in the upper troposphere.

In order to better understand the adiabatic dynamics in our numerical experiments, we first conducted the experiments in a dry mode. The absence of moisture in the dry experiments simplifies the dynamics of the simulated weather system, and in that way helps to elucidate the consequences of the environmental temperature changes without the effect of latent heat release. Dry integrations are used in idealized simulations, for example when studying the boundary-layer characteristics of mid-latitude cyclones (Sinclair et al, 2010; Boutle et al, 2010). Some studies have also been done with dry initial conditions, but allowing moisture to enter the atmosphere through the surface fluxes during the simulation (e.g. Boutle et al, 2011; Booth et al, 2013). In our dry cases, however, the atmosphere was kept dry throughout the whole integration. This was done by turning off the cloud microphysics and cumulus convection, and switching off the surface moisture fluxes. After that, similar experiments were performed with moisture. These moisture-including simulations are hereafter called "MOIST", and "DRY" refers to simulations done without moisture. Note that in both dry and moist simulations, the surface sensible heat and momentum fluxes were on all the time.

Table 1 Notation in the energy metrics.

$[\,]$	zonal mean
$*$	deviation from the zonal mean
$\langle\,\rangle$	area mean
$"$	deviation from the area mean
c_p = 1004 J kg^{-1}	specific heat of dry air at constant volume
$\mathbf{F}$	friction force per unit mass
g = 9.81 m s^{-2}	gravitational acceleration
p	pressure
p_{TOP}	upper boundary of the model domain
p_0 = 1000 hPa	lower boundary of the analysis domain
p_T = 100 hPa	upper boundary of the analysis domain
R = 287 J kg^{-1}	gas constant of dry air
T	temperature
$\mathbf{V}$	horizontal wind vector
α	specific volume
$\gamma = \frac{R}{c_p p}(\frac{p_0}{p})^{\kappa}(-\frac{\partial\langle\theta\rangle}{\partial p})^{-1}$	stability parameter
$\kappa = R/c_p$	kappa parameter
θ	potential temperature
$\omega = \frac{dp}{dt}$	isobaric vertical motion

2.3 Cyclone energetics

To shed light on the mechanisms by which the changes in temperature affect the cyclone development, more in-depth analysis of the cyclone energetics was conducted. To this end, time series of different energy quantities for each experiment, and for both dry and moist simulations were calculated. The values of the energy quantities are area-averaged and integrated over the whole air column, thus representing the state of the whole model domain. Furthermore, only the most important parts of the atmospheric energy cycle in terms of mid-latitude cyclone dynamics are analysed in this paper. A complete list of atmospheric energy components and conversion terms can be found from Boer and Lambert (2008). The equations were derived originally by Lorenz (1955) and Oort (1964). The notation in the following equations is conventional and the symbols are listed in Table 1.

The available potential energy of the zonal mean flow (A_Z) is calculated as follows:

$$\langle A_Z \rangle = \int_{p_T}^{p_0} \frac{1}{2} c_p \gamma \left\langle [T]^{"2} \right\rangle \frac{dp}{g}. \quad (3)$$

A_Z acts as a source of energy for the baroclinic wave, and therefore decreases with time. The corresponding eddy available potential energy A_E

$$\langle A_E \rangle = \int_{p_T}^{p_0} \frac{1}{2} c_p \gamma \left\langle T^{*2} \right\rangle \frac{dp}{g} \quad (4)$$

represents the potential energy that can be further converted to eddy kinetic energy K_E:

$$\langle K_E \rangle = \int_{p_T}^{p_0} \frac{1}{2} \left\langle \left| \mathbf{V}^* \right|^2 \right\rangle \frac{dp}{g}. \quad (5)$$

The conversion terms between the mentioned energy quantities are also calculated. The conversion between A_Z and A_E ($C(A_Z,A_E)$), which is usually positive in the atmosphere, is given by:

$$C\Big(\langle A_Z\rangle,\langle A_E\rangle\Big) = -\int_{p_T}^{p_0} c_p\gamma\Big\langle [T^*v^*]\frac{\partial T}{\partial y}\Big\rangle\frac{dp}{g} - \int_{p_T}^{p_0} c_p\gamma\Big(\frac{p}{p_0}\Big)^{\kappa}\Big\langle [T^*\omega^*]"\frac{\partial[\theta]"}{\partial p}\Big\rangle\frac{dp}{g}. \quad (6)$$

This means that the eddy is receiving potential energy from the zonal mean flow, which occurs when the meridional heat flux is directed towards lower temperatures, i.e. the cyclone acts to reduce temperature differences in the meridional direction but increase them in the zonal direction. Furthermore, A_E can be converted to K_E through the sinking of relatively cold air and the rising of warm air in the eddy:

$$C\Big(\langle A_E\rangle,\langle K_E\rangle\Big) = -\int_{p_T}^{p_0}\Big\langle \alpha^*\omega^*\Big\rangle\frac{dp}{g}. \quad (7)$$

Finally, the dissipation of K_E by friction and turbulence is calculated as follows:

$$\langle D_E\rangle = -\int_{p_T}^{p_0}\Big\langle \mathbf{V}^*\cdot\mathbf{F}^*\Big\rangle\frac{dp}{g}. \quad (8)$$

Before going to the results of our experiments, we need to pay attention to one technicality of A_Z. As will be discussed in Section 3, the inclusion of moisture reduces A_Z. This is because we held the air density the same between the corresponding dry and moist simulations. Thus, with the same density, the run with moisture needs to be slightly colder, particularly in the southern part of the model domain where the moisture content is larger. Consequently, the meridional temperature gradient at lower levels is slightly stronger in dry simulations. Note that although the air density was fixed between dry and moist simulations, it was changed between CTRL and the different temperature experiments.

The energy equations used in our analyses are all for a dry atmosphere, which means that they are not fully accurate for the moist waves. In particular, the amount of A_Z may differ largely between moist and dry atmospheres, and can also show opposite sensitivity to increased atmospheric temperature (Kirshbaum et al, 2018). However, as the calculation of A_Z for moist flows is not a straightforward task (Stansifer et al, 2017), we acknowledge this limitation of our analyses and leave it for a potential further investigation.

As a last note, only the results of the T_0 = 6 K runs are shown in Section 3. The differences in the responses between the T_0 = 2, 4 and 6 K runs are in most cases sufficiently linear, and thus showing only the T_0 = 6 K run serves the purpose. These T_0 = 6 K runs of Experiments UNI, LOW and UP are denoted in the text as UNI6, LOW6 and UP6. However, the corresponding figures for the T_0 = 2 and 4 K runs are included in Section S1.2 of the supplementary material.

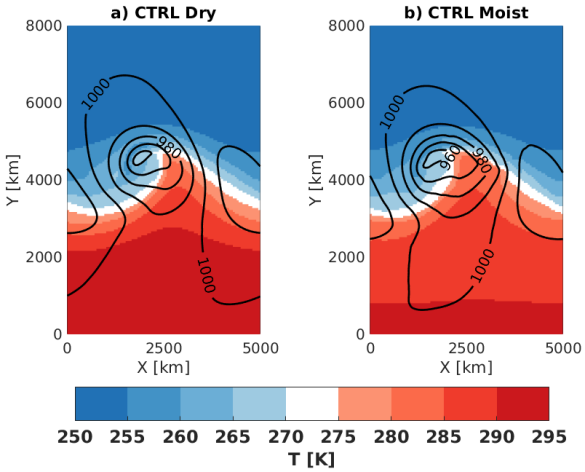

Fig. 2 Surface pressure (contours) and 850 hPa temperature (colors) in a) DRY-CTRL and b) MOIST-CTRL at t = 5 days

3 Results

Figure 2 gives a snapshot of the structure of the cyclone in DRY-CTRL and MOIST-CTRL, 5 days after the start of the simulation. The cyclone without moisture (Fig. 2a) has 1.3 hPa higher central surface pressure compared to the one with moisture (Fig. 2b). This difference in their intensities is still growing, reaching 7.4 hPa at their deepest stage (see Table 2 for the numerical values). This is because diabatic heating, dominated by latent heat release, acts as a deepening mechanism in this idealized baroclinic wave simulation, which was diagnosed with height tendency equation in Rantanen et al (2017). However, in both simulations the initial disturbance develops eventually to a very typical, text-book type extra-tropical cyclone.

Figure 3 shows the time evolution of minimum surface pressure (hereafter SP_{min}) and K_E for both DRY-CTRL and MOIST-CTRL, and for the T_0 = 6 runs of the experiments. Firstly, besides being deeper (compare Fig. 3a and 3b), the cyclones formed in a moist environment clearly have also more kinetic energy (compare Fig. 3c and 3d) than the ones formed in a dry environment. Furthermore, the response to the temperature forcings is greater in the moist simulations, as there is more variation in minimum of SP_{min} and maximum of K_E.

The numerical values of SP_{min} and K_E at two different times are given in Table 2. The values for the three temperature experiments are given as differences relative to the relevant CTRL run (e.g. DRY-CTRL or MOIST-CTRL). In

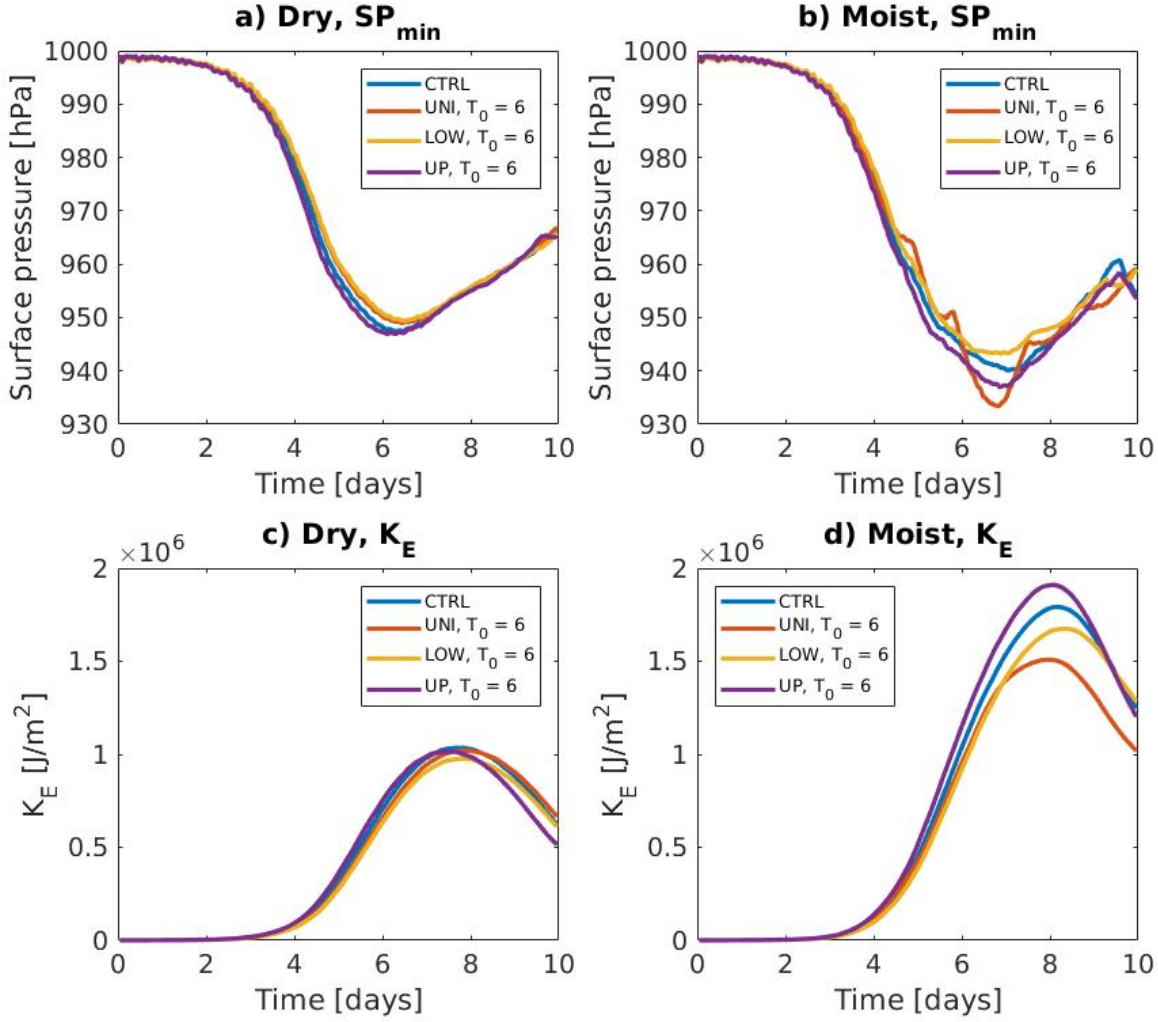

Fig. 3 Time evolution of a) the minimum surface pressure in the dry experiments, b) the minimum surface pressure in the moist experiments, c) eddy kinetic energy in the dry experiments and d) eddy kinetic energy in the moist experiments. In addition to CTRL, only the $T_0 = 6$ K runs from each experiment are included

the table, the SP_{min} and K_E values at $t = 5$ days are used as a proxy for the initial deepening rate and the K_E growth rate of the cyclone, respectively. In addition, the minimum of SP_{min} and maximum of K_E are given. It is important to consider both the rate of change and the peak values when studying the intensity of cyclones.

The uniform increase of temperature by 6 K in the dry atmosphere slows down the deepening of the cyclone by 2.4 hPa during the first 5 days (Table 2). This difference in the depth is slightly reduced when the deepest stage of the low is reached, being then only 1.5 hPa. In line with these SP_{min} values, DRY-UNI6 has less K_E than DRY-CTRL both during the deepening stage and at the mature stage of the cyclone.

In DRY-LOW6, the response is similar to but slightly larger than that in DRY-UNI6: both the deepening rate and the maximum intensity are reduced when the lower level temperature gradient is decreased (see Table 2). Finally, in DRY-UP6, the upper level temperature gradient was increased, which slightly accelerates the deepening and the K_E growth rate of the cyclone during the first 5 days (Table 2). However, even though the cyclone remains marginally (by 0.6 hPa) deeper than in DRY-CTRL at the deepest stage, it actually contains less kinetic energy when its maximum intensity is reached. We will analyze the causes of this unintuitive behaviour later, in Section 3.3.

In MOIST-UNI6, the surface low is 4.8 hPa shallower than in MOIST-CTRL at $t = 5$ days, but still reaches a 6.8 hPa lower minimum pressure at the mature stage. This is due to enhanced diabatic processes, as will be discussed in Section 3.1. Furthermore, the kinetic energy of MOIST-UNI6 stays constantly below MOIST-CTRL, as also seen from Fig. 3d (red line). Similarly as in the dry simulation,

Table 2 SP_{min} and K_E at $t = 5$ days and the minimum of SP_{min} and maximum of K_E during the 10-day simulations. The results for the T_0 = 6 K runs of the three experiments are shown as differences from the control run values. The values at $t = 5$ days can be used as a proxy for the initial growth rate whereas the minimum/maximum values reflect the maximum intensity of the cyclone. The unit for SP_{min} is *hPa* and that for K_E $10^5\ Jm^{-2}$.

Run	SP (5 days)	SP (min)	K_E (5 days)	K_E (max)
Dry CTRL	957.5	947.5	3.2	10.3
Dry UNI6 - CTRL	2.4	1.5	-0.33	-0.15
Dry LOW6 - CTRL	2.8	1.9	-0.48	-0.58
Dry UP6 - CTRL	-1.7	-0.6	0.39	-0.19
Moist CTRL	956.2	940.1	4.5	18
Moist UNI6 - CTRL	4.8	-6.8	-0.25	-2.8
Moist LOW6 - CTRL	1.9	3.1	-0.64	-1.2
Moist UP6 - CTRL	-3.4	-3.1	0.66	1.2

the cyclone in MOIST-LOW6 is weaker than the cyclone in MOIST-CTRL. This is a direct consequence of the weakened baroclinicity and holds true with all the SP_{min} and K_E measures in Table 2. Lastly, the increase of upper tropospheric temperature gradient in the moist atmosphere induces 3.4 hPa / 5 days faster cyclogenesis, with the eventual minimum value being 3.1 hPa below MOIST-CTRL. In contrast with the dry simulation, the maximum value of K_E in MOIST-UP6 exceeds that in MOIST-CTRL (see also Fig. 3d, violet line).

3.1 Experiment UNI: uniform temperature increase (dry + moist)

In DRY-UNI6, the cyclone formed in a 6 K warmer environment is slightly weaker than in DRY-CTRL (see Table 2 and the red lines in Fig. 3a and Fig. 3c). This modest weakening of the cyclone with the warming is related to the weakening of the jet stream and thus baroclinicity with the warming (Fig. 1d). This is because the uniform warming of the atmosphere increased pressure relatively more in the northern side of the domain, which weakened the meridional pressure gradient and thus also decelerated the geostrophic wind speed. The reduction of the baroclinicity is visible also in Fig. 4a where the T_0 = 6 run (red dashed line) has less A_Z compared to the control run (blue dashed line).

Diabatic processes become important when moisture enters the simulations. The warming of the whole domain by 6 K raises the atmospheric moisture content, which then materializes as an increased latent heat release in the vicinity of the surface low. This enhanced diabatic heating results in the surface low reaching a lower minimum pressure than in MOIST-CTRL (Fig. 5). However, the deepening does not occur steadily. Fig. 5 shows that the rapid deepening periods starting on days 5 and 6 coincide with increased diabatic heating above the surface low (Fig. 5, red line). During the last deepening period, on day 6, the centre of surface low in MOIST-UNI6 is located near the occlusion point of the cyclone (Fig. 6d), which differs noticeably from MOIST-CTRL (Fig. 6c). Thus, these separate deepening periods are due to localized, small-scale features which intensified consecutively within the surface low. Similar type of rapid reintensification of the surface low was found in Boutle et al (2010). They attribute this to a localized spin-up near the surface caused by the latent heat release.

Nevertheless, even though the uniform warming of the environment by 6 K in the moist case produces the deepest surface low in our experiments, this cyclone actually has the lowest maximum K_E of all the moist experiments, including MOIST-CTRL (Table 1 and Fig. 3d). This is because the localized minima of surface pressure, induced by latent heat release, are so small scale features that they have very little effect on the domain-averaged K_E (Boutle et al, 2010). Figure 4a shows that MOIST-UNI6 has less A_Z (red solid line) than MOIST-CTRL (blue solid line) in the beginning of the simulation. Moreover, the cyclone in MOIST-UNI6 also does not exploit A_Z as efficiently as the one in MOIST-CTRL, due to weaker $C(A_Z, A_E)$ (Fig. 4d). For this reason, MOIST-UNI6 has more A_Z left in the end of the simulation than MOIST-CTRL.

Kirshbaum et al (2018) studied closely the production of K_E in their warmed and moistened simulations, and found that the warm-frontal updraft strengthens and migrates progressively eastwards when temperature is increased. For this reason, the area of updraft coincides less well with the warm sector, and thereby the baroclinic production of K_E can be hindered. Although they increased the temperature more (from 275 K to 290 K in the middle of the domain) than what is done in our simulations (from 279 K to 285 K), our results seem to confirm this outcome. This can be seen from Fig. 6. On day 5, MOIST-UNI6 has two separate ascent maximums (Fig. 6b), while in MOIST-CTRL, the frontal ascent is located more evenly along the warm front. For this reason, less rising motion is taking place within the warm sector (indicated as red lines in Fig 6) in MOIST-UNI . Moreover, and consistent with the findings of Kirshbaum et al (2018), the ascent in MOIST-UNI6 on day 5 and 6 extends further east, occurring more outside of the warm sector. Therefore, the phasing between ω^* and $\alpha^*(=RT^*/p^*)$ weakens, which indicates reduced $C(A_E, K_E)$ according to Eq. (7).

The reason why A_E in MOIST-UNI6 also experiences such a major reduction (-25 % in maximum value compared to MOIST-CTRL, solid lines in Fig. 4b) remains partially unclear for us. However, similar results were shown by Tierney et al (2018) who found that eddy available potential energy decreased when surface temperature in the middle of the domain increased above 276.5 K. Based on their results, the reduction of A_E with the warming originated from decreased $C(A_Z, A_E)$, which is consistent with our results. By

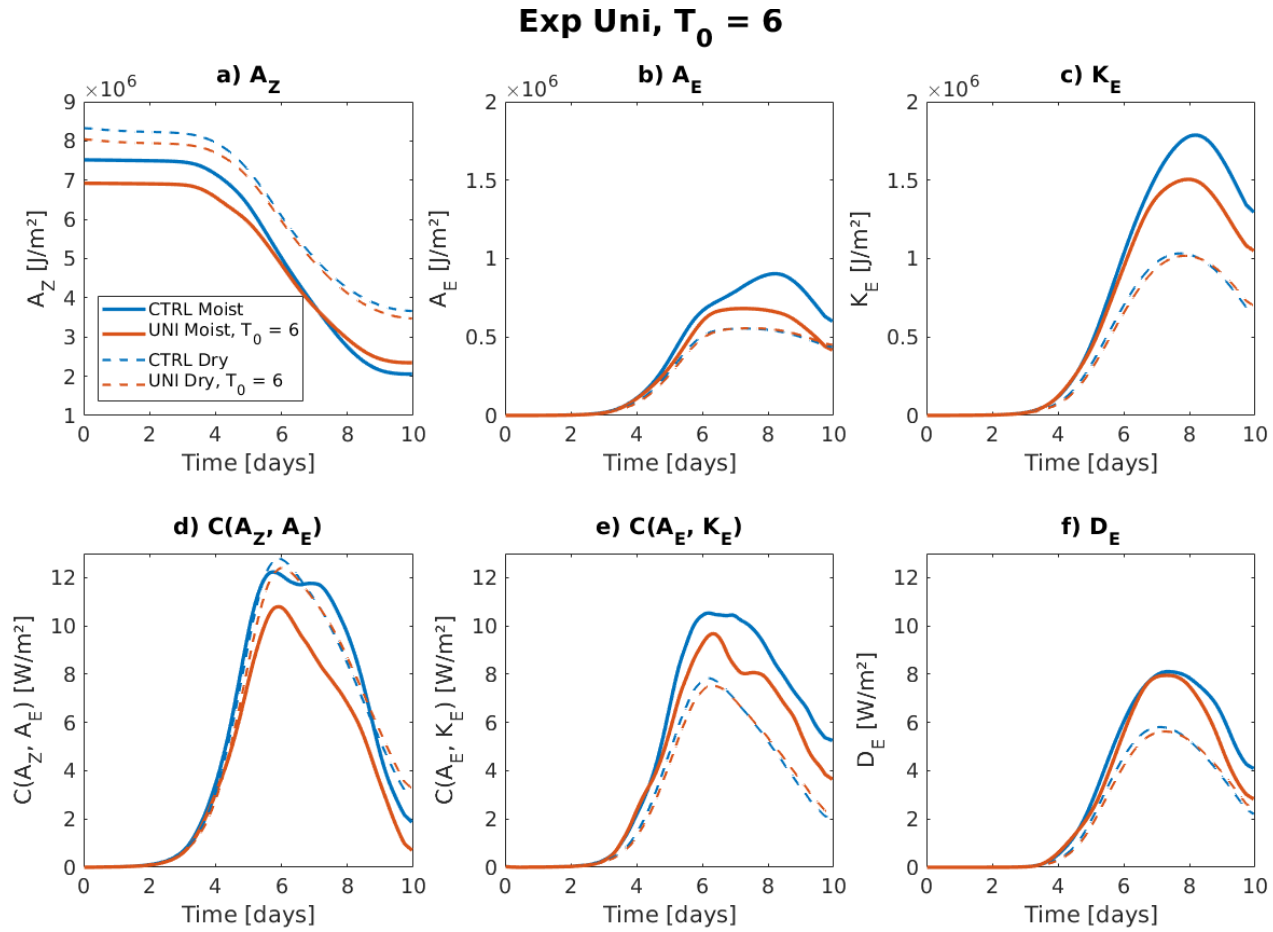

Fig. 4 Time evolution of a) available potential energy of the zonal mean flow (A_Z), b) available potential energy of the eddy (A_E), c) kinetic energy of the eddy (K_E), d) energy conversion from A_Z to A_E, e) energy conversion from A_E to K_E and f) eddy kinetic energy dissipation. In all of the panels, blue dashed line is DRY-CTRL and red dashed line is DRY-UNI6. The solid lines are the same, but for moist simulations. Unit for the energy terms (a–c) is Jm^{-2} and that for the conversion terms (d–f) Wm^{-2}

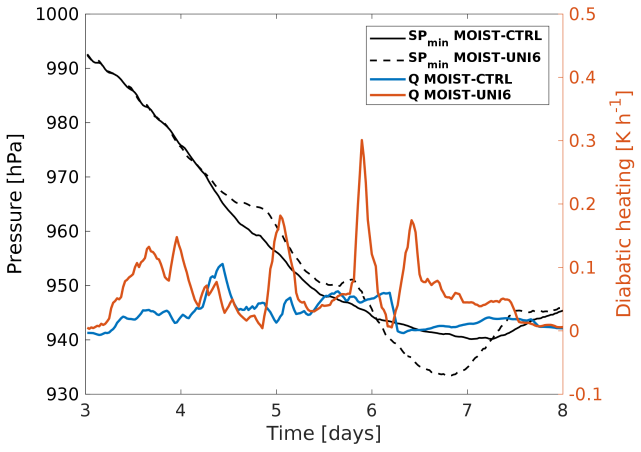

Fig. 5 Time evolution of the minimum surface pressure in MOIST-CTRL (black solid line) and MOIST-UNI6 (black dashed line), and vertically averaged diabatic heating in MOIST-CTRL (blue line) and MOIST-UNI6 (red line) from an area of 350 km x 350 km centered at the surface pressure minimum. The time series of diabatic heating are smoothed by 2-hour moving average

contrast, the findings of Kirshbaum et al (2018) are somewhat inconsistent: in their study, the tendency of A_E is not noticeably dependent on temperature (Fig. 17a in their paper), which differs from Fig. 4b of our study, and Fig. 8a of Tierney et al (2018). In any case, one explanation for this reduction of A_E could be that the weakening of winds associated with the weaker production of K_E reduces the meridional heat flux induced by the eddy, which then appears as a lower maximum of A_E later on, at day 8. Nevertheless, the decreased $C(A_Z,A_E)$ combined with the fact that the cyclone in MOIST-UNI6 has initially less A_Z leads to the situation where the cyclone in MOIST-UNI6 has less A_E compared to MOIST-CTRL.

Booth et al (2013) and Tierney et al (2018) found that the horizontal scale of the cyclone also tends to decrease with increased moisture content in the atmosphere. Thus, they suggest that this contraction of the storm is intimately related to the decrease of K_E. In our simulations, when raising the temperature 6 K from MOIST-CTRL, the meridional extent of the storm seems to decrease slightly (compare po-

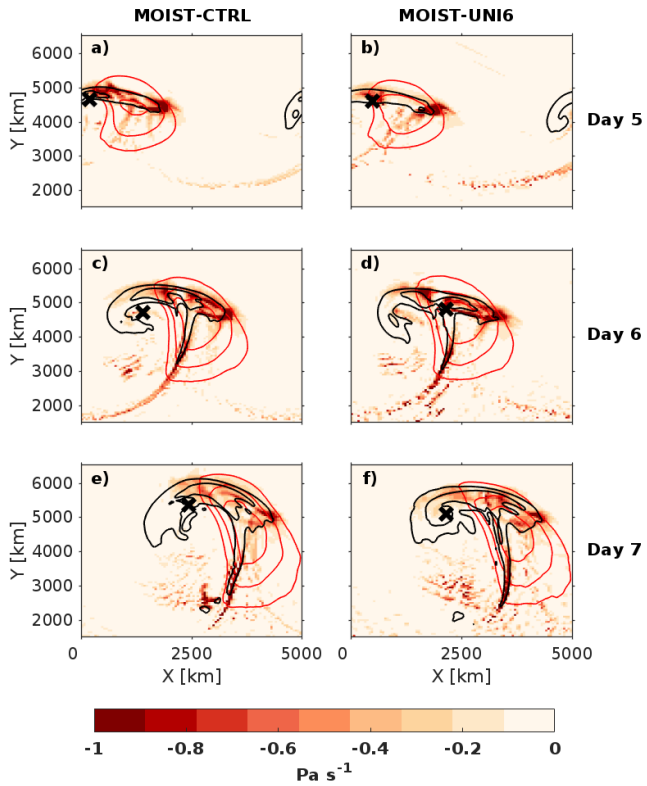

Fig. 6 500-900 hPa mean ω (colours, only negative values shown), 500-900 hPa mean T^* (red contours for 5, 9 and 13 K values) and 700-900 hPa Ertel PV (black contours for 1 and 2 PVU) for MOIST-CTRL (left) and MOIST-UNI6 (right) on day 5, 6 and 7. The cross marks the location of the surface low

tential vorticity (hereafter PV) anomalies in Fig. 6e and 6f). In addition, Booth et al (2013) and Tierney et al (2018) found that the maximum of K_E responds non-monotonically to increasing atmospheric moisture. Their results indicate that the amount of K_E increases significantly when moisture is added from dry to normal conditions. Beyond that, the increase of absolute moisture actually starts to reduce the maximum K_E. This is consistent with our results (Fig. 4c) as well; K_E increases considerably when the moisture is included (cf. blue dashed and solid lines in Fig. 4c), but then decreases when the moisture is further increased (blue solid and red solid lines in Fig. 4c).

3.2 Experiment LOW: decrease of lower level temperature gradient (dry + moist)

The time series of SP_{min} and K_E of Experiment LOW are presented with yellow lines in Fig. 3. In this experiment, the low level meridional temperature gradient was decreased. The results are largely as expected: the cyclone remains weaker, regardless if moisture is present or not. The decrease in baroclinicity is explicit in Fig. 7a: both simulations show $\sim$ 10 % a reduction of the initial A_Z. Why the modification of the lower tropospheric temperature gradient has such a clear impact on A_Z and consequently the development of the cyclone is partly explained by the vertical distribution of A_Z. The northward decrease in temperature (and therefore A_Z) in these experiments, and in the Northern Hemisphere in general, is strongest near the surface; this makes the reduction of the initial temperature gradient to occur at the levels where A_Z reaches its maximum. For this reason, even a small change in the temperature gradient in the lower troposphere can have a large impact on the total amount of A_Z.

The mechanisms of the weakening can be traced further by studying the energetics of the cyclone: Fig. 7 shows that the maximum values of all energy components and conversion terms are systematically smaller in the T_0 = 6 K run than in the control runs. Although the changes in the moist simulations (solid lines) are somewhat larger, the sign of the T_0 = 6 K runs relative to the control runs are qualitatively similar in both dry and moist simulations, which increases the robustness of the result.

3.3 Experiment UP: increase of upper level temperature gradient (dry + moist)

As Table 2 reveals, the increase of baroclinicity in the upper troposphere does not increase the maximum K_E in DRY-UP6. In fact, K_E in DRY-UP6 exceeds DRY-CTRL at $t = 5$ days (Table 2), but the maximum of K_E remains actually lower (see also Fig. 8c, dashed lines). In other words, the kinetic energy starts to increase faster, but the cyclone decays earlier. However, the situation changes when moisture is present: the kinetic energy increases (Fig. 3d and Fig. 8c, solid lines) and the surface low also becomes notably deeper (Fig. 3b). Thus, in the more realistic case where the moisture is included, increasing the upper level temperature gradient leads to a more intense life cycle.

Because the results of the DRY-UP simulations were somewhat against our initial hypothesis, we studied in more detail the energetics of this experiment. To shed light on the changes in the dynamics of the cyclone, we first need to consider the dashed lines in Fig. 8a. Naturally, A_Z is greater in DRY-UP6 than in DRY-CTRL due to the increase in the upper level temperature gradient. Despite the larger storage of A_Z, however, the maximum of A_E (Fig. 8b, dashed lines) and the maximum of K_E (Fig. 8c, dashed lines) remain lower compared to DRY-CTRL. In other words, the cyclone in DRY-UP6 has seemingly more favourable initial conditions, but it cannot exploit as much of the potential energy in theory available from the zonal mean flow and thus stays weaker.

One reason for the weaker ability of the cyclone to exploit the increased baroclinicity is related to the fact that the temperature gradient was only increased in the upper troposphere. There, the acceleration of zonal wind speed (Fig. 1f)

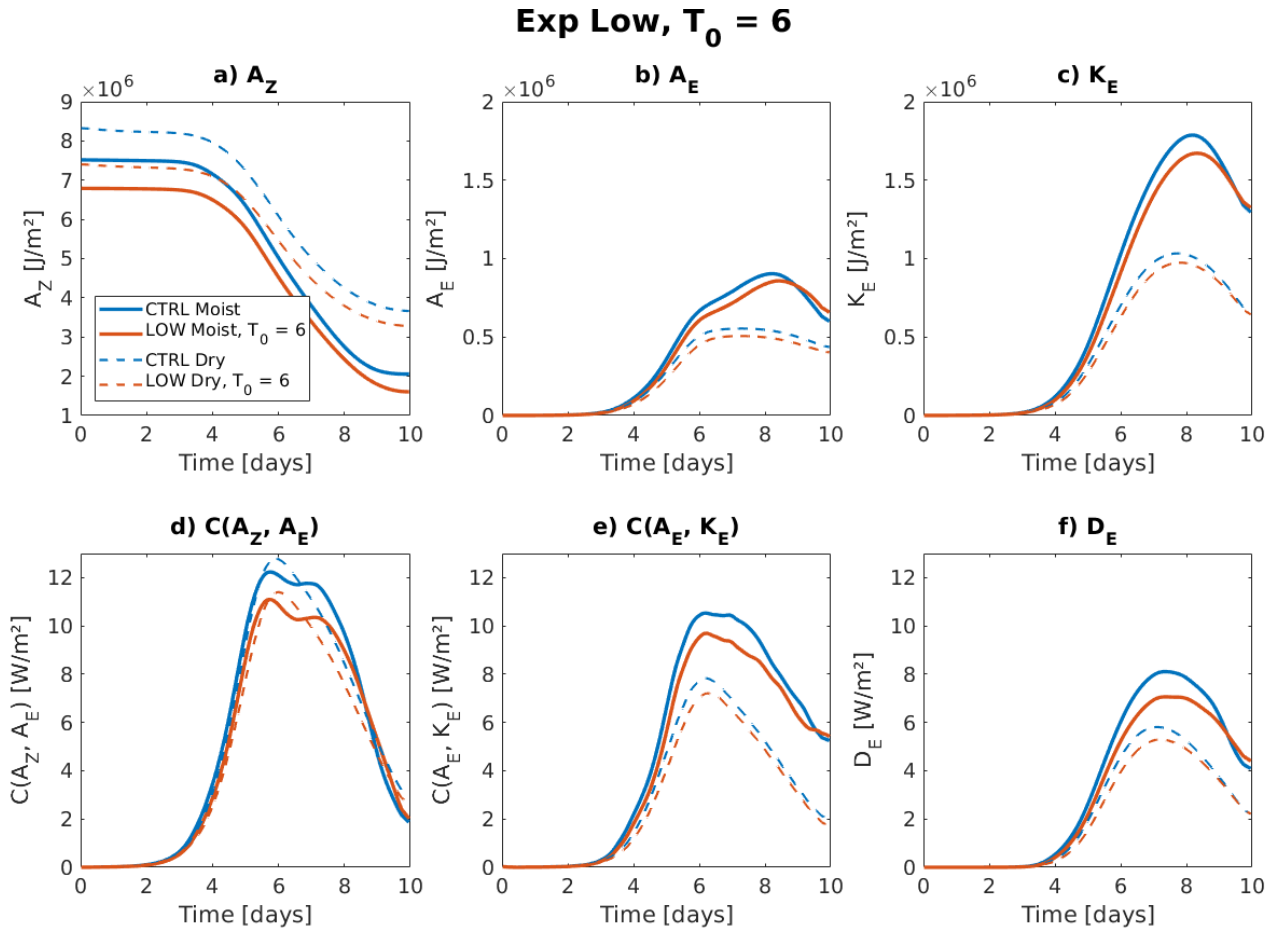

Fig. 7 As Fig. 4, but for Experiment LOW.

induces faster development of the surface low, which is also seen as slightly lower values of SP_{min} during the deepening phase at $t = 5$ days (Table 2). This marginally stronger cyclogenesis, due to the positive anomaly of A_Z in the upper troposphere, leads to a faster consumption of A_Z also in the lower troposphere (not shown). However, since DRY-UP6 does not have a larger storage of A_Z to be utilized in the lower troposphere, this faster conversion makes the amount of lower tropospheric A_Z in DRY-UP6 decrease faster compared to DRY-CTRL.

Figure 8d (dashed lines) shows the time evolution of $C(A_Z,A_E)$ in DRY-UP6. Beginning from day 6, the conversion is weaker than in DRY-CTRL, because a larger part of the lower tropospheric storage of A_Z has already been consumed by that time DRY-UP6. Although the difference is quite small, the reduced energy conversion after day 6 is most likely the main reason behind the lower maximum of A_E and K_E in DRY-UP6 compared to DRY-CTRL.

$C(A_Z,A_E)$ in the atmosphere is largely dominated by the meridional heat flux in the eddy (the first term on the right-hand side of Eq. 6). By only taking into account this first term of the conversion equation, and using the fact that the correlation between T^* and v^* is defined as

$$r(T^*v^*) = \frac{[T^*v^*]}{\sigma_{T^*}\sigma_{v^*}}, \tag{9}$$

we can rewrite the conversion as follows:

$$C_{xyz}\Big(\langle A_Z\rangle, \langle A_E\rangle\Big) \approx -\int_0^{p_0} c_p\gamma\left\langle r(T^*v^*)_x(\sigma_{T^*}\sigma_{v^*})_y\frac{\partial T}{\partial y}_z\right\rangle\frac{dp}{g}. \tag{10}$$

Here the covariance $[T^*v^*]$ has been substituted with the product of the correlation $r(T^*v^*)$ and standard deviations $(\sigma_{T^*}\sigma_{v^*})$ of the named variables. The subscript x, y or z refers either to the DRY-CTRL $(x,y,z = 0)$ or DRY-UP6 $(x,y,z = 1)$. Thus, Eq. 10 can be used for investigating the conversion in more detail: we can calculate how $C(A_Z,A_E)$ changes when only some factors from DRY-UP6 are present in the calculation of $C(A_Z,A_E)$. The value of γ in Eqs. 10–13 is from DRY-CTRL.

The blue line in Fig. 9a presents the conversion which has been calculated by using the values of DRY-CTRL $(x,y,z =$

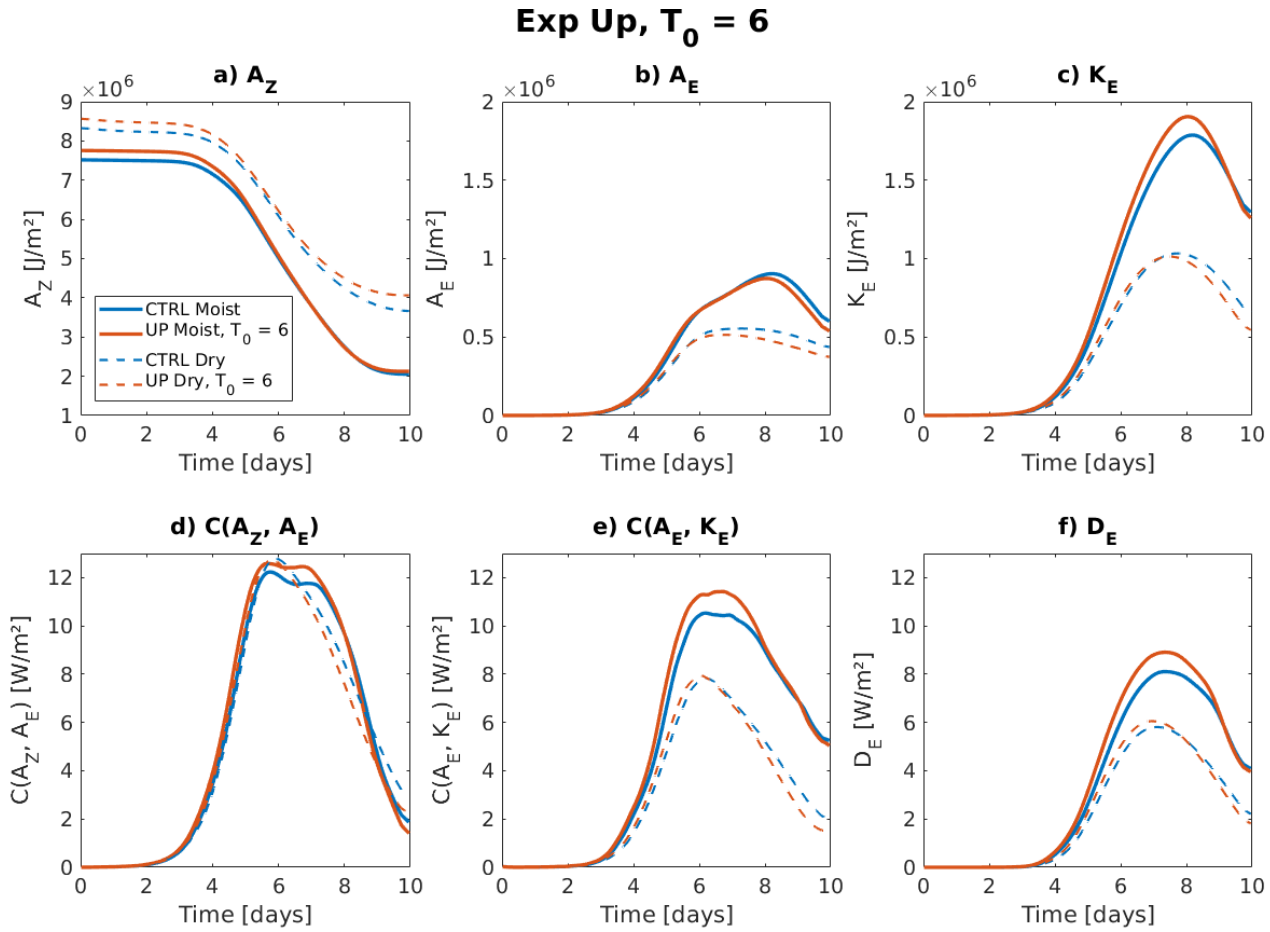

Fig. 8 As Fig. 4, but for Experiment UP

0):

$$C_{000}\Big(\langle A_Z\rangle,\langle A_E\rangle\Big)\approx -\int_0^{p_0} c_p\gamma\Big\langle r(T^*v^*)_0(\sigma_{T^*}\sigma_{v^*})_0\frac{\partial T}{\partial y}_0\Big\rangle\frac{dp}{g}. \quad (11)$$

To study how much the intensity of the cyclone alone affects the conversion, the standard deviations of temperature and meridional wind speed in Eq. 11 have been replaced by the values from DRY-UP6 ($y=1$, $x,z=0$), while keeping the stability, the correlation between temperature and meridional wind speed, and the meridional temperature gradient at their values in DRY-CTRL:

$$C_{010}\Big(\langle A_Z\rangle,\langle A_E\rangle\Big)\approx -\int_0^{p_0} c_p\gamma\Big\langle r(T^*v^*)_0(\sigma_{T^*}\sigma_{v^*})_1\frac{\partial T}{\partial y}_0\Big\rangle\frac{dp}{g}. \quad (12)$$

This conversion C_{010} is shown with the red line in Fig. 9a. By comparing this with C_{000} (blue line), we can see that C_{010} at its maximum is ~ 9 % more efficient, on day 5. Hence, if the temperature gradient was unchanged, the conversion by the cyclone in DRY-UP6 would be initially larger simply because the cyclone develops faster and becomes stronger earlier. See also the anomaly relative to DRY-CTRL in Fig. 9d (solid line).

In Fig. 9b, the conversion depicted with the red line has been calculated in the same manner as in Fig. 9a, but now the meridional temperature gradient has been taken from DRY-UP6 and the other parameters from DRY-CTRL ($z=1$, $x,y=0$):

$$C_{001}\Big(\langle A_Z\rangle,\langle A_E\rangle\Big)\approx -\int_0^{p_0} c_p\gamma\Big\langle r(T^*v^*)_0(\sigma_{T^*}\sigma_{v^*})_0\frac{\partial T}{\partial y}_1\Big\rangle\frac{dp}{g} \quad (13)$$

Surprisingly, the conversion C_{001} would be weaker on days 4–7 (Fig. 9d, dashed line) regardless of the increased upper tropospheric temperature gradient. This weakened conversion originates from the lower troposphere. The temperature gradients at lower levels are initially similar in both runs, but due to the more rapid cyclogenesis in DRY-UP6 the low-level baroclinicity is consumed faster. This is the reason for the weakened conversion during days 4–7 in Fig. 9b (see also the dashed line in Fig. 9d).

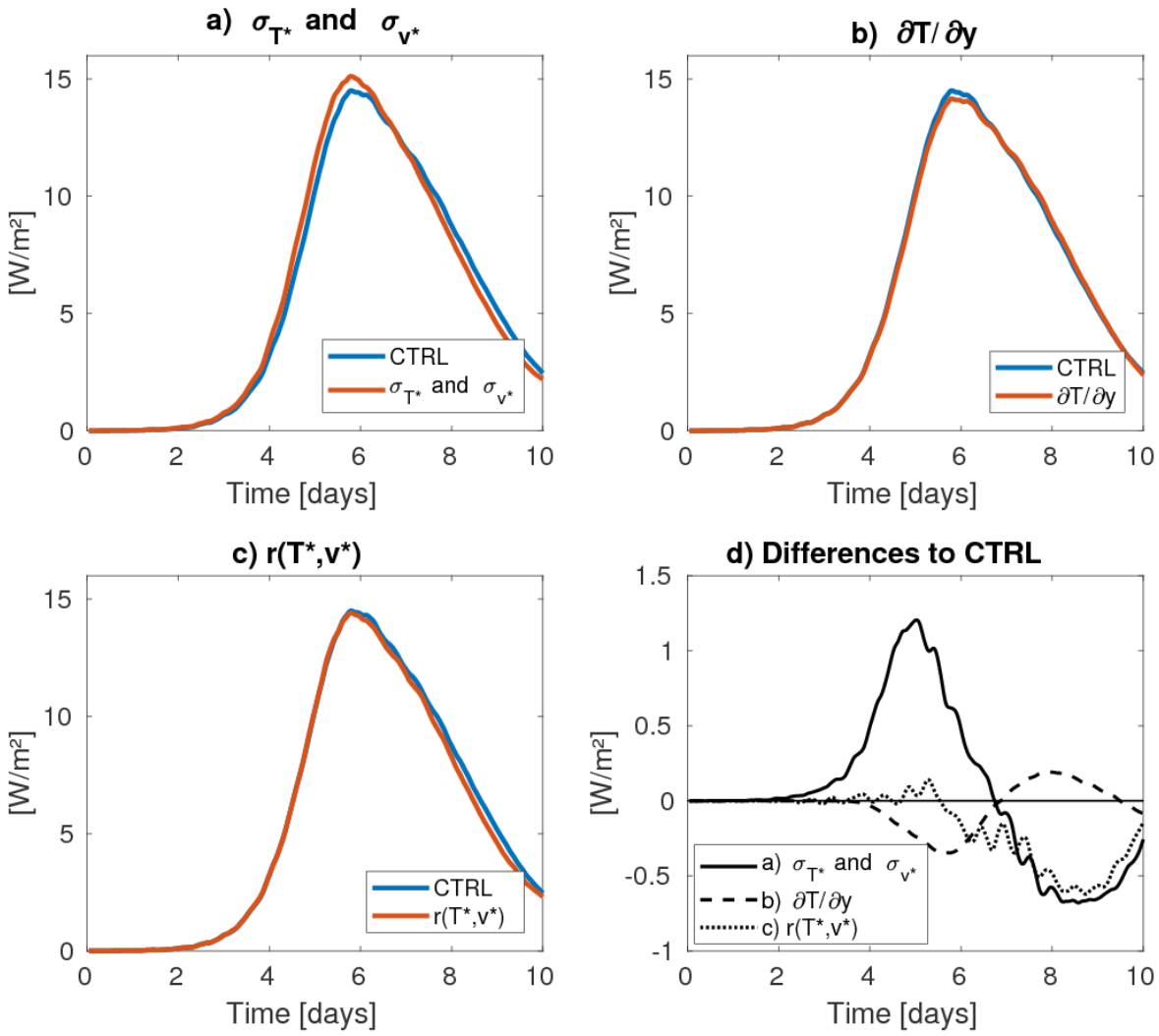

Fig. 9 The effect of different factors on energy conversion from A_Z to A_E. In the calculation of the conversion term in Eq. 10 (red line), only the named factors have been taken from DRY-UP6: a) standard deviations of temperature and meridional wind speed, b) meridional temperature gradient, and c) correlation between temperature and meridional wind speed. The other factors are from DRY-CTRL. For full explanation of the method, see Sec. 3.3. Finally, in d), the anomalies of a), b) and c) relative to the control run (blue line) are shown

The final factor affecting $C(A_Z,A_E)$ is the phasing between the temperature and wind fields. This reflects the structure of the disturbance: the more closely the area of relatively warm (cold) air matches with the area of southerly (northerly) wind, the more effective the meridional heat flux and thus the conversion is. This factor is represented by the correlation $r(T^*,v^*)$ in Eq. (6). Thus, the conversion with the red line in Fig. 9c has been calculated by taking $r(T^*,v^*)$ from DRY-UP6 but the other parameters from DRY-CTRL. Clearly, the effect of $r(T^*,v^*)$ on the conversion remains very small until day 6, but after that the weakening of the correlation starts to decrease the energy conversion.

As a summary of Fig. 9, the retardation of the fast development in DRY-UP6 originates from the weakened $C(A_Z,A_E)$. This reduced energy transfer is first due to a loss of baroclinicity in the lower troposphere (Fig. 9b), and slightly later also due to unfavorable phasing between temperature and wind fields (Fig. 9c). The unfavorable phasing is ultimately because of the increased wind speed in the upper troposphere (Fig. 1f), which disturbs the vertical structure of the cyclone. Furthermore, the trough axis is more vertically aligned in DRY-UP6 than in DRY-CTRL after day 4 (not shown). According to Hoskins et al (1985), too strong upper-level winds can disrupt the phase-locking and sustained growth of a synoptic-scale disturbance whose amplitude is initially small. This also seems to be the case in the DRY-UP6. Finally, after day 7, the weakening of the disturbance itself starts to decrease its energy production (Fig. 9a). As the net effect of all these three factors, the decrease in K_E starts ear-

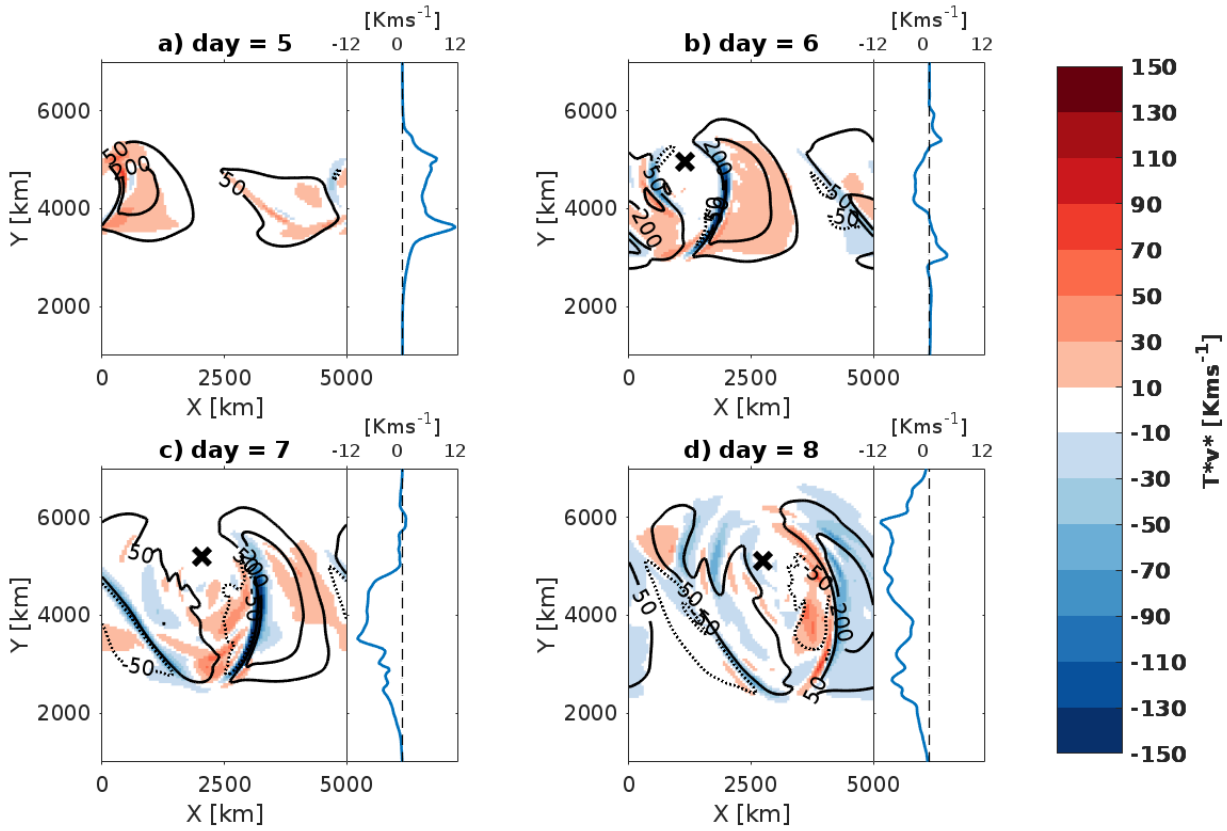

Fig. 10 T^*v^* (contours) and its difference to the control run (colours) at the 600 hPa level in DRY-UP6, at a) day 5, b) day 6, c) day 7 and d) day 8. Zonal means of the T^*v^* differences are shown next to each map with blue line. In the maps, solid lines depict positive T^*v^* values (contours for 50, 200 and 400 Kms^{-1}) while negative values are shown with dashed lines (-50 Kms^{-1} contour). The cross marks the location of the surface low. When calculating the difference between DRY-UP6 and DRY-CTRL, the T^*v^* fields have been shifted so that the surface lows from both runs are aligned in x-direction

lier in DRY-UP6 than in DRY-CTRL and the maximum of K_E is slightly lower.

To get a more concrete understanding of the weakening $C(A_Z,A_E)$ in DRY-UP6, T^*v^* maps of the T_0 = 6 K run and their differences to DRY-CTRL at 600 hPa are shown in Fig. 10 for four different times. Furthermore, the zonal means of the differences are depicted to the right of each map. On day 5, the meridional heat flux T^*v^* is generally larger in DRY-UP6 (map of Fig. 10a) than in DRY-CTRL, which is mostly due to higher v^* in DRY-UP6. This makes the conversion stronger (sum of Fig. 9a and Fig. 9c). However, on day 6, the meridional heat flux starts to become weaker than in DRY-CTRL, decreasing first around the centre of the surface low (Fig. 10b). After that, on days 7 and 8, the zonal mean of the meridional heat flux ($[T^*v^*]$) becomes $\sim$ 5-10 K ms^{-1} weaker than in DRY-CTRL (Fig. 10c and 10d, blue lines), which means a $\sim$ 15–20 % reduction in relative terms (not shown). This reduction in $[T^*v^*]$ originates from the narrow area on the western edge of the warm sector (map of Fig. 10c). Another visible feature in the maps is the reduction of the positive (red) $[T^*v^*]$ anomaly within the warm sector, which ends up being negative (blue) on day 8 (Fig. 10d). The decrease in the warm-sector heat flux is consistent with the overall weakening of the cyclone relative to DRY-CTRL, and starts to weaken $C(A_Z,A_E)$ compared to DRY-CTRL after day 6.

In MOIST-UP6, the maximum of A_E (Fig. 8b, solid lines) remains lower than in MOIST-CTRL, whereas K_E (Fig. 8c, solid lines) peaks notably higher. The higher maximum of K_E is due to more effective conversion from A_E to K_E (Fig. 8e, solid lines). Figure 11 shows the meridional averages (from 2000 to 6000 km in y-direction) of diabatic heating and PV* in DRY-UP6 and MOIST-UP6. DRY-UP6 does not contain moisture, thus the only contribution to diabatic heating comes from the boundary-layer dissipation and surface heat fluxes. In any case, the upper level winds in both DRY-UP6 and MOIST-UP6 are increased relative to corresponding CTRL runs, hence implying faster eastward propagation of the upper level PV anomalies. We suggest the following explanation for why the increased upper-level baroclinicity leads to an increase in K_E in MOIST-UP6 despite a decrease in DRY-UP6. In MOIST-UP6, diabatic heating

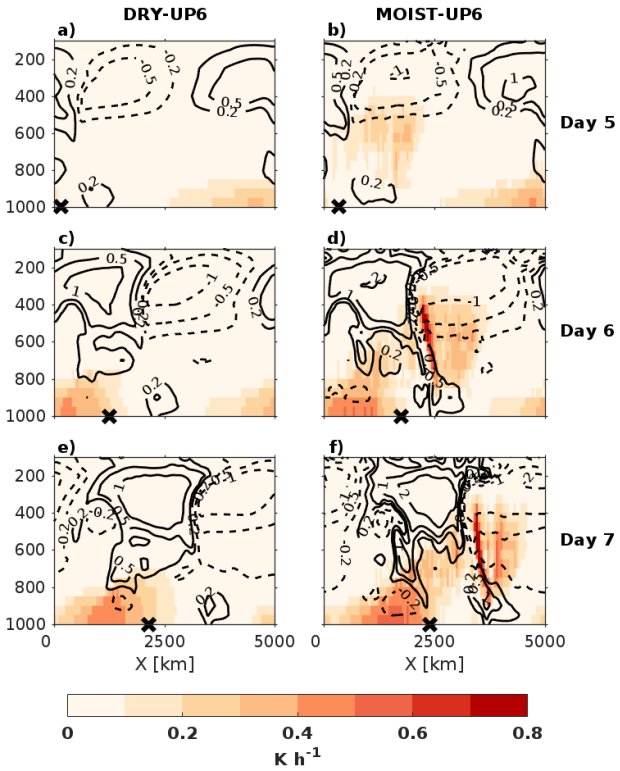

Fig. 11 Meridionally averaged cross sections of diabatic heating (colours) and Ertel PV departure from the zonal mean (contours, positive values in solid lines, negative values in dashed lines) in DRY-UP6 (left) and MOIST-UP6 (right) on day 5, 6 and 7. The meridional average has been taken over 2000 km to 6000 km in y-direction of the domain. The cross marks the location of the surface low

extends up to the height of upper level PV anomalies ($\sim$ 300 hPa level) (Fig. 11d and 11f). Thus, the heating helps to connect the upper- and low-level PV anomalies via the generation of low-level PV below the heating maximum. For example, in MOIST-UP6, as the upper level wind speeds are increased, the propagation speed of the heating maximums and thus the propagation speed of low-level PV generation increase accordingly. In addition, the heating enhances the negative PV anomaly and divergence aloft, which restricts the forward propagation of the positive PV anomaly associated with the upper trough. This whole process allows the cyclone to exploit more effectively the increased baroclinicity in the upper troposphere, which is seen as higher maximums of $C(A_Z,A_E)$ (Fig. 8d) and $C(A_E,K_E)$ (Fig. 8e) compared to MOIST-CTRL. However, this mechanism is not present in DRY-UP6 (Fig. 11c and 11e), where the phase-locking between upper and lower levels can break more easily if the upper level winds are increased too much.

4 Discussion

In order to identify the changes in adiabatic dynamics of the cyclones, all experiments were conducted first in a dry atmosphere. Naturally, this can raise a reasonable question: why focus on the effects in a dry atmosphere, as the results are not directly applicable to the real, moist atmosphere? Our answer is that the scope of this study is to identify the mechanisms by which modified temperature distributions affect the dynamics of mid-latitude cyclones. In this context, idealized dry simulations provide a valuable benchmark, although they clearly must be complemented by more realistic moist simulations.

Our results don't necessarily apply to all baroclinic waves. As found in Kirshbaum et al (2018), the sensitivity of K_E to larger temperatures can be reversed using a different jet stream in the model initialization. In addition, the surface type and the wavelength may also affect the sensitivity. However, as these caveats found by Kirshbaum et al (2018) affect the production of K_E, which is strongly dependent on the distribution of diabatic heating in the eddy, they are only directly applicable to the MOIST-UNI experiment. In the LOW and UP experiments instead, where the magnitude of diabatic heating was not changed significantly compared to corresponding CTRL runs, the changes in cyclone intensity are mainly related to the changed baroclinicity. Therefore, the results of the LOW and UP experiments might be more universal amongst various baroclinic waves, but of course more experiments are needed to confirm this.

Finally, although the temperature changes investigated in this study will occur simultaneously in the real atmosphere, investigating their effects on mid-latitude cyclogenesis separately will help to understand and interpret e.g. the results of climate change projections made with GCMs. Nevertheless, one topic for additional studies would be to apply all three temperature modifications together, like they will occur in the real world. That would help to assess the linearity of the cyclone dynamics to the performed temperature changes. This is an important issue when drawing conclusions from our results to real-world changes in mid-latitude cyclones in a changing climate.

5 Conclusions

We investigated the response of extra-tropical cyclones to different atmospheric temperature changes: 1) uniform temperature increase, 2) decrease of the lower level meridional temperature gradient and 3) increase of the upper level temperature gradient. These temperature forcings are incorporated to the initial state of the idealised model experiments one at a time. Hence, this method allows one to identify how extra-tropical cyclones respond to changes in the environmental temperature distribution and ascertain the underlying responsible physical mechanisms. The main tool for identifying the changes in the simulated weather systems is an energy cycle analysis, which is carried out for each model experiment.

Increasing the temperature and thus moisture content in the atmosphere from typical present-day values induces deeper cyclones with less amplified upper-level dynamic properties, such as eddy kinetic energy. This decrease of eddy kinetic energy with the warming is in line with recent studies by Kirshbaum et al (2018) and Tierney et al (2018), but contrary to Boutle et al (2011). In addition, Kirshbaum et al (2018) did not observe the decrease of minimum surface pressure, which can be partly explained by the coarser horizontal grid spacing (Δx = 100 km) used in their simulations. According to Kirshbaum et al (2018), the reduction of eddy kinetic energy with warming can be traced further to be a consequence from unfavourable phasing between rising motion and buoyancy within the warm sector. This is also confirmed by our results. Furthermore, and similarly to Kirshbaum et al (2018), the warming of the cyclone environment uniformly decreases the capability of the cyclone to utilize the available potential energy from the zonal mean flow.

The main outcome emerging from our temperature gradient experiments is that the cyclone responds differently to the changes in lower and upper level gradients. The decrease of lower level meridional temperature gradient, a scenario expected with climate change in Northern mid-latitudes, is found to decrease the strength of the storm in a straightforward way: all the energy quantities used in this paper remain lower regardless whether moisture is present in the simulation or not. This is a direct outcome from the decreased baroclinicity.

The increase of the upper level temperature gradient, also a scenario expected in a warmer climate, however, is found to affect the development of the cyclone in a more complex way. In the dry atmosphere, increasing the upper level temperature gradient decreases the eddy kinetic energy, whereas in the moist atmosphere the kinetic energy of the cyclone increases. The increase of baroclinicity in the upper troposphere boosts the jet stream considerably, which induces stronger cyclogenesis and thereby faster consumption of the potential energy in the lower troposphere. This leads eventually to a loss of conversion from the available potential energy of the zonal mean flow to eddy potential energy during the mature stage, and consequently a premature decay of the storm. However, due to latent heat release, the response in the moist atmosphere is different: diabatic heating enhances the interaction between upper- and low-level PV anomalies, and hence helps the surface cyclone to exploit the increased upper level baroclinicity. As a result, the kinetic energy of the cyclone increases at larger meridional temperature gradients in the upper troposphere, when moisture is present.

Acknowledgements MR acknowledges the Doctoral Programme in Atmospheric Sciences (ATM-DP, University of Helsinki) for financial support. This work was partially funded by the Academy of Finland Center of Excellence programme (project no. 307331). The authors wish to acknowledge CSC – IT Center for Science, Finland, for computational resources. The authors thank also Daniel Kirshbaum and three other anonymous reviewers for their insightful and constructive comments.

References

Bengtsson L, Hodges KI, Roeckner E (2006) Storm tracks and climate change. J Climate 19:3518–3543

Bengtsson L, Hodges KI, Keenlyside N (2009) Will extratropical storms intensify in a warmer climate? J Climate 22:2276–2301

Blázquez J, Pessacg NL, Gonzalez PL (2013) Simulation of a baroclinic wave with the wrf regional model: sensitivity to the initial conditions in an ideal and a real experiment. Meteorol Appl 20:447–456

Boer G, Lambert S (2008) The energy cycle in atmospheric models. Clim Dynam 30:371–390

Booth JF, Wang S, Polvani L (2013) Midlatitude storms in a moister world: lessons from idealized baroclinic life cycle experiments. Clim Dynam 41:787–802

Boutle I, Beare R, Belcher SE, Brown A, Plant RS (2010) The moist boundary layer under a mid-latitude weather system. Bound-Lay Meteorol 134:367–386

Boutle I, Belcher S, Plant R (2011) Moisture transport in midlatitude cyclones. Q J Roy Meteor Soc 137:360–373

Catto JL, Shaffrey LC, Hodges KI (2011) Northern Hemisphere extratropical cyclones in a warming climate in the HiGEM high-resolution climate model. J Climate 24:5336–5352

Fantini M (2004) Baroclinic instability of a zero-PVE jet: Enhanced effects of moisture on the life cycle of midlatitude cyclones. J Atmos Sci 61:1296–1307

Fink AH, Brücher T, Ermert V, Krüger A, Pinto JG (2009) The European storm Kyrill in January 2007: synoptic evolution, meteorological impacts and some considerations with respect to climate change. Nat Hazard Earth Sys 9:405–423

Hong SY, Dudhia J, Chen SH (2004) A revised approach to ice microphysical processes for the bulk parameterization of clouds and precipitation. Mon Weather Rev 132:103–120

Hong SY, Noh Y, Dudhia J (2006) A new vertical diffusion package with an explicit treatment of entrainment processes. Mon Weather Rev 134:2318–2341

Hoskins BJ, McIntyre M, Robertson AW (1985) On the use and significance of isentropic potential vorticity maps. Q J Roy Meteor Soc 111:877–946

Kain JS, Fritsch JM (1993) Convective parameterization for mesoscale models: The kain-fritsch scheme. In: The representation of cumulus convection in numerical models, Springer, pp 165–170

Kirshbaum DJ, Merlis T, Gyakum J, McTaggart-Cowan R (2018) Sensitivity of idealized moist baroclinic waves to environmental temperature and moisture content. J Atmos Sci 75:337–360

Lambert SJ, Fyfe JC (2006) Changes in winter cyclone frequencies and strengths simulated in enhanced greenhouse warming experiments: results from the models participating in the IPCC diagnostic exercise. Clim Dynam 26:713–728

Lorenz EN (1955) Available potential energy and the maintenance of the general circulation. Tellus 7:157–167

O'Gorman PA (2011) The effective static stability experienced by eddies in a moist atmosphere. J Atmos Sci 68:75–90

Oort AH (1964) On estimates of the atmospheric energy cycle. Mon Weather Rev 92:483–493

Paulson CA (1970) The mathematical representation of wind speed and temperature profiles in the unstable atmospheric surface layer. J Appl Meteorol 9:857–861

Pfahl S, Ogorman PA, Singh MS (2015) Extratropical cyclones in idealized simulations of changed climates. J Climate 28:9373–9392

Rantanen M, Räisänen J, Lento J, Stepanyuk O, Räty O, Sinclair VA, Järvinen H (2017) OZO v. 1.0: software for solving a generalised omega equation and the Zwack–Okossi height tendency equation using WRF model output. Geosci Model Dev 10:827–841

Shamarock W, Klemp J, Dudhia J, Gill D, Barker D, Duda M, Huang X, Wang W, Powers J (2008) A description of the advanced research WRF version 3. NCAR technical note NCAR/TN/u2013475

Sinclair VA, Keyser D (2015) Force balances and dynamical regimes of numerically simulated cold fronts within the boundary layer. Q J Roy Meteor Soc 141:2148–2164

Sinclair VA, Belcher SE, Gray SL (2010) Synoptic controls on boundary-layer characteristics. Bound-Lay Meteorol 134:387–409

Solomon S (2007) Climate change 2007 - the physical science basis: Working group I contribution to the fourth assessment report of the IPCC, vol 4. Cambridge University Press

Stansifer EM, O'Gorman PA, Holt JI (2017) Accurate computation of moist available potential energy with the Munkres algorithm. Q J Roy Meteor Soc 143:288–292

Tierney G, Posselt DJ, Booth JF (2018) An examination of extratropical cyclone response to changes in baroclinicity and temperature in an idealized environment. Clim Dynam pp 1–18

Waite ML, Snyder C (2009) The mesoscale kinetic energy spectrum of a baroclinic life cycle. J Atmos Sci 66:883–901

Wernli H, Dirren S, Liniger MA, Zillig M (2002) Dynamical aspects of the life cycle of the winter storm Lothar (24–26 December 1999). Q J Roy Meteor Soc 128:405–429

Whitaker JS, Davis CA (1994) Cyclogenesis in a saturated environment. J Atmos Sci 51:889–908

Woollings T (2008) Vertical structure of anthropogenic zonal-mean atmospheric circulation change. Geophys Res Lett 35(19)

Yin JH (2005) A consistent poleward shift of the storm tracks in simulations of 21st century climate. Geophys Res Lett 32(18)

Zappa G, Shaffrey LC, Hodges KI, Sansom PG, Stephenson DB (2013) A multimodel assessment of future projections of North Atlantic and European extratropical cyclones in the CMIP5 climate models. J Climate 26:5846–5862